



Insights into vertical differences of particle number size distributions in winter in Beijing, China

Wei Du^{a,b}, Weigang Wang^c, Ranran Liu^a, Yuying Wang^d, Yingjie Zhang^a, Jian Zhao^b, Lubna Dada^b, Conghui Xie^a, Qingqing Wang^a, Weiqi Xu^a, Wei Zhou^a, Fang Zhang^e, Zhanqing Li^e, Pingqing Fu^f, Jie Li^a, Juha Kangasluoma^b, Zifa Wang^a, Maofa Ge^c, Markku Kulmala^{b,g,h}, Yele Sun^{a,i,*}

^a State Key Laboratory of Atmospheric Boundary Layer Physics and Atmospheric Chemistry, Institute of Atmospheric Physics, Chinese Academy of Sciences, Beijing 100029, China

^b Institute for Atmospheric and Earth System Research/Physics, University of Helsinki, P.O. Box 64, Helsinki 00014, Finland

^c State Key Laboratory for Structural Chemistry of Unstable and Stable Species, Institute of Chemistry, Chinese Academy of Sciences, Beijing 100190, China

^d School of Atmospheric physics, Nanjing University of Information Science and Technology, Nanjing 210044, China

^e College of Global Change and Earth System Science, Beijing Normal University, Beijing 100875, China

^f Institute of Surface-Earth System Science, Tianjin University, Tianjin 300072, China

^g Joint International Research Laboratory of Atmospheric and Earth System Sciences, School of Atmospheric Sciences, Nanjing University, Nanjing, China

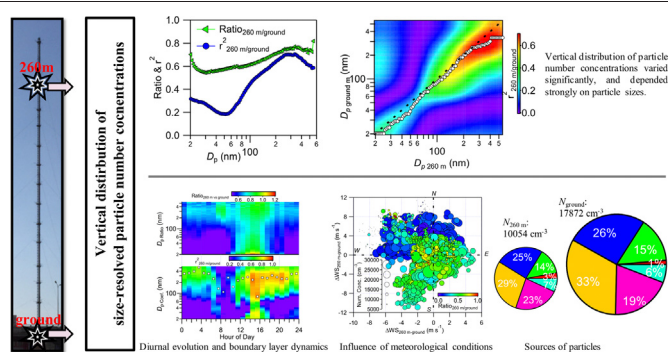
^h Aerosol and Haze Laboratory, Beijing Advanced Innovation Center for Soft Matter Science and Engineering, Beijing University of Chemical Technology, Beijing, China

ⁱ Center for Excellence in Regional Atmospheric Environment, Institute of Urban Environment, Chinese Academy of Sciences, Xiamen 361021, China

HIGHLIGHTS

- First simultaneous winter measurements of particle number size distributions at ground level and city aloft in urban Beijing.
- Vertical differences of particle number concentrations varied significantly as a function of particle size.
- Boundary layer dynamics, meteorology, local and regional sources are major factors driving vertical changes.

GRAPHICAL ABSTRACT



ARTICLE INFO

Article history:

Received 5 May 2021

Received in revised form 19 July 2021

Accepted 11 August 2021

Available online 19 August 2021

Editor: Jianmin Chen

Keywords:

Particle number size distribution

Vertical distribution

Temperature inversion

ABSTRACT

Particle number size distribution (PNSD) is of importance for understanding the mechanisms of particle growth, haze formation and climate impacts. However, the measurements of PNSD aloft in megacities are very limited. Here we report the first simultaneous winter measurements of size-resolved particle number concentrations along with collocated gaseous species and aerosol composition at ground level and 260 m in Beijing. Our study showed that the vertical differences of particle number concentrations between ground level and aloft varied significantly as a function of particle size throughout the study. Further analysis illustrated the impacts of boundary dynamics and meteorological conditions on the vertical differences of PNSD. In particular, the temperature and relative humidity inversions were one of the most important factors by decoupling the boundary layer into different sources and processes. Positive matrix factorization analysis identified six sources of PNSD at both ground level and city aloft. The local source emissions dominantly contributed to Aitken-mode particles, and showed the largest vertical gradients in the city. Comparatively, the regional particles were highly correlated between ground

* Corresponding author at: State Key Laboratory of Atmospheric Boundary Layer Physics and Atmospheric Chemistry, Institute of Atmospheric Physics, Chinese Academy of Sciences, Beijing 100029, China.

E-mail address: sunyele@mail.iap.ac.cn (Y. Sun).

Source apportionment
Beijing

level and city aloft, and the vertical differences were relatively stable throughout the day. Our results point towards a complex vertical evolution of PNSD due to the changes in boundary layer dynamics, meteorological conditions, sources, and processes in megacities.

© 2021 Elsevier B.V. All rights reserved.

1. Introduction

High concentration of atmospheric particles in populated urban areas is one of the major environmental concerns because of its profound influences on visibility and human health (Zhang et al., 2015). The particle number size distribution (PNSD) is critical in determining these effects. For example, the size-dependent light scattering of particles is the major factor for visibility impairment (Seinfeld and Pandis, 2016). Compared with the direct aerosol effects including scattering and absorbing radiation, aerosol particles also exert influences on climate indirectly by influencing cloud properties, and particle diameter is considered to be critical for cloud-nucleating ability (Dusek et al., 2006). Moreover, evidence shows that the toxicity of aerosol particles depends on particle size, and smaller particles (e.g., < 100 nm) are more toxic than those in larger sizes (Seaton et al., 1995). Thus, extensive studies have been performed to characterize PNSDs worldwide, promoting a better understanding of PNSD in various environments including their sources, chemistry and their impacts on human health and climate (Kulmala et al., 2004).

PNSD has also been widely studied in China, including Beijing-Tianjin-Hebei region (Gao et al., 2012; Shen et al., 2016; Zhou et al., 2020), Yangtze River Delta (Peng et al., 2014; Wang et al., 2014), and Pearl River Delta (Yue et al., 2013; Yue et al., 2010) regions. As the capital of China and a rapidly developing megacity, Beijing faces severe haze pollution problems and attracts extensive studies. However, the relationship of PNSD and air pollution in Beijing is still controversial. Previous studies showed a shift of PNSD to large sizes in polluted events, and hence the growth of small particles may play an important role in haze formation (Du et al., 2021; Guo et al., 2014; Kulmala et al., 2021; Yue et al., 2009). Thus, investigating the dynamic evolution of PNSDs will help interpret the formation mechanisms of haze pollutions in Beijing.

PNSD varied largely in different seasons due to the influences of meteorological conditions, boundary layer evolution, and emission sources in Beijing (Wu et al., 2008). Temperature (T) dependent processes in atmosphere were found to mostly affect particles smaller than 100 nm (Olivares et al., 2007). Comparatively, the number concentrations of Aitken mode and accumulation mode particles decreased as the increase of wind speed (WS), while that of nucleation mode particles increased (Lang et al., 2013). This observation is related to new particle formation (NPF) which is associated with the decrease in condensation sink resulting from decreased Aitken and accumulation mode particles (Kulmala et al., 2021; Zhou et al., 2020). In addition, particle number concentrations were often found to be high when the relative humidity (RH) was high in Beijing (Zhang et al., 2001), and RH also affected PNSD substantially due to hygroscopic growth (S. Huang et al., 2010; Zhang et al., 2001). Recently, positive matrix factorization (PMF) of PNSD was used to investigate the sources of particles, and the results showed that the number of small particles can be affected significantly by local emissions, e.g., traffic and cooking emissions (Cai et al., 2020; Liu et al., 2016; Liu et al., 2014; Wang et al., 2013). Therefore, measurements of PNSD aloft in the city are needed to better understand the relative contributions of regional transport and local emissions to aerosol particles. For instance, Du et al. (2017) conducted the first simultaneous measurements of size-resolved particle number concentrations at ground level and 260 m in urban Beijing, and the results showed that local cooking emissions contributed to small particles substantially at ground level while the contributions were much smaller at 260 m. However, our

understanding of vertical distributions of PNSDs in Beijing is far from complete, especially in winter with frequent haze events.

In this study, we conducted simultaneous measurements of PNSDs at 260 m and ground level on the Beijing 325 m meteorological tower (BMT) in winter 2016 using two same scanning mobility particle sizers (SMPS). The vertical differences of size-resolved particle number concentrations between ground level and city aloft are characterized, and the causes for the vertical differences with e.g., boundary layer (BL) and meteorological conditions are explored. Also, the sources of size-resolved aerosol particles are analysed with positive matrix factorization, and the contributions of local emissions and regional transport to the vertical differences are demonstrated.

2. Experimental methods

2.1. Sampling site and instruments

The sampling site is located at the Tower Branch of Institute of Atmospheric Physics, Chinese Academy of Sciences between the north third and fourth ring roads in Beijing (Du et al., 2021). The PNSDs were measured using two scanning mobility particle sizers (SMPS) that are equipped with long Differential Mobility Analyzer (DMA, TSI, 3081A) and Condensation Particle Counter (CPC, models 3775 at ground level and 3772 at 260 m, respectively). Aerosol particles in the size range of 14–685 nm at 260 m, and 11–552 nm at ground level were measured simultaneously with different flow rates (0.3 L min⁻¹ vs. 1 L min⁻¹). In addition, an Aerodyne high-resolution time-of-flight aerosol mass spectrometer (HR-ToF-AMS) and an aerosol chemical speciation monitor (ACSM) were deployed to measure submicron aerosol (PM₁) species including organics (Org), sulfate (SO₄), nitrate (NO₃), ammonium (NH₄), chloride (Cl) at ground level and 260 m, respectively (Xu et al., 2019), and two seven-wavelength Aethalometers (AE33, Magee Scientific Corp.) were used to measure equivalent black carbon (BC) (Xie et al., 2019). Besides, collocated measurements at the two heights included CO, SO₂, and O₃. Aerosol particles were dried to RH below 40% using silica gel diffusion dryers during the measurements. To ensure the stability of the sampling flow, we cleaned the orifice and the sampling line regularly. A more detailed description of the operation and maintenance of the instruments was described in Du et al. (2021). The meteorological parameters including RH , T , WS , and wind direction (WD) at 15 heights were measured on the BMT. As shown in Fig. S1, the average temperature was 1.7 °C at 260 m and 3.6 °C at ground level during the entire period. Frequent temperature and RH inversions were observed in this study, leading to significant differences in PM₁ mass concentrations at the two heights (64.7 μg m⁻³ at 260 m vs. 83.4 μg m⁻³ at ground level).

2.2. Data analysis

Before the campaign, the measurements of the two SMPSs were first compared at ground site for two days to evaluate the uncertainties due to the different instruments. As shown in Fig. S2, the PNSDs measured by the two SMPSs agreed well while the ratio of PNSDs indicated some differences, especially for particles smaller than 20 nm (Ratio < 0.6). Further, the size-resolved correction coefficient calculated as the ratio of average PNSD from the two SMPSs during the inter-comparison period was applied to the two datasets obtained at two heights (Fig. S3a).

As shown in Fig. S3, the reconstructed PNSDs agreed excellently between the two SMPSs including the number concentrations in three different modes, e.g., particles in the size range of 100 to 550 nm ($N_{100-550}$), 30 to 100 nm (N_{30-100}) and 20 to 30 nm (N_{20-30}). Considering the large uncertainty of particles smaller than 20 nm, the reconstructed PNSDs in the size range from 20 nm to 550 nm were used in this study.

2.3. Source apportionment of size-resolved particle number concentrations

To investigate the potential particle sources, we performed positive matrix factorization (PMF2.exe, v 4.2) (Paatero and Tapper, 1994; Ulbrich et al., 2009) analysis. Using an equation-based approach according to Ogulei et al. (2007), the measurement uncertainties (Unc) were estimated by Eq. (1)

$$\text{Unc}_{ij} = \sigma_{ij} + C_1 \times X_{ij} \quad (1)$$

where C_1 is a constant value assumed to be 0.1; X_{ij} is the measured particle number concentration; and σ_{ij} is the estimated measurement errors calculated using Eq. (2)

$$\sigma_{ij} = C_2 \times (X_{ij} + \bar{X}_j) \quad (2)$$

where C_2 is a constant value assumed to be 0.01; \bar{X}_j is the arithmetic mean value for j th size bin. To compare sources at the two heights, the size-resolved particle number concentration at the two heights were combined together for PMF analysis. In total, six factors were chosen, and the diagnostics of PMF results are presented in Fig. S4.

Besides, PMF analysis were also performed to organic aerosol (OA) measured by HR-ToF-AMS. Three primary OA (POA) from fossil fuel-related OA (FFOA), cooking OA (COA) and biomass burning OA (BBOA), and three secondary OA (SOA) namely, oxidized POA (OPOA), oxygenated OA (OOA), and aqueous-phase OOA (aq-OOA), were reported in Xu et al. (2019).

3. Results and discussion

3.1. Overview of PNSDs

Fig. 1 shows the average PNSDs at 260 m and ground level for the entire study. The average number concentration at ground level in the size range of 20–550 nm was $17,878 \pm 8376 \text{ cm}^{-3}$, which was 76% higher than that reported in autumn ($10,134 \pm 4680 \text{ cm}^{-3}$) (Du et al., 2017). Although the average number concentration was 44% lower at 260 m ($10,065 \pm 5190 \text{ cm}^{-3}$) compared to ground level, it was still 35% higher than that observed in autumn ($7473 \pm 4324 \text{ cm}^{-3}$) (Du et al., 2017). The bimodal mode fitting showed that the particles at 260 m were dominated by the small mode (72%), while at ground level the contributions of the two modes were comparable (52% vs. 48%). As demonstrated by the frequency histogram in Fig. 1b, the probability of particle number concentration exceeding $20,000 \text{ cm}^{-3}$ was only 4% at 260 m while 40% at ground level, suggesting a more severe particle pollution at ground level.

Further analyses showed that the ratios ($\text{Ratio}_{260 \text{ m}/\text{ground}}$) and correlation coefficients ($r_{260 \text{ m}/\text{ground}}^2$) of particle number concentrations between two heights depended strongly on particle

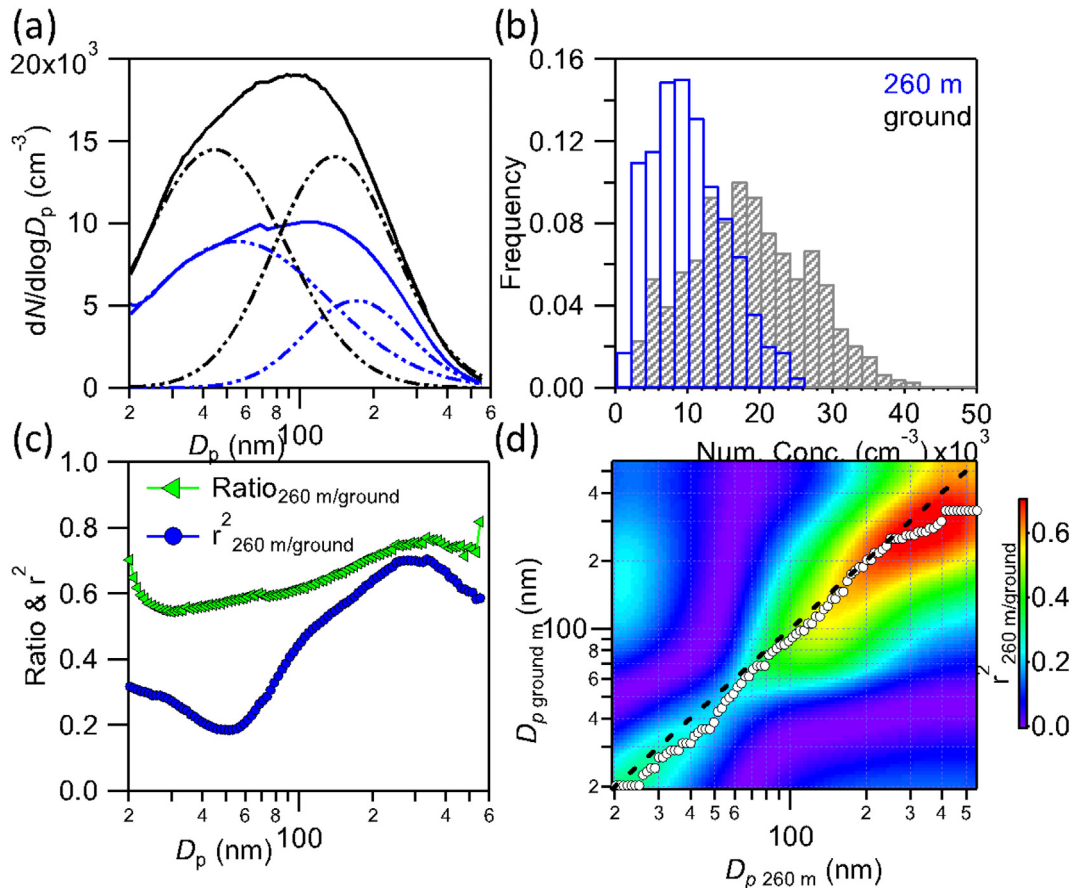


Fig. 1. Characterizations of vertical differences of particle number size distributions. (a) Average particle number size distributions (solid line) and bimodal fitted particle number size distributions (dashed line), and (b) frequency as a function of particle number concentration at 260 m and ground level, respectively. (c) shows the ratio ($\text{Ratio}_{260 \text{ m}/\text{ground}}$) and correlation coefficient ($r_{260 \text{ m}/\text{ground}}^2$) of particle number concentrations at 260 m to those at ground level as a function of particle size. (d) Correlation coefficients ($r_{260 \text{ m}/\text{ground}}^2$) between 260 m and ground level of each size bin. The white dots represent the best correlations.

size (Figs. 1 and S5). Fig. 1c shows the $\text{Ratio}_{260\text{ m/ground}}$ calculated from the average PNSDs in Fig. 1a and $r_{260\text{ m/ground}}^2$ based on the time series of number concentration in each size bins. $r_{260\text{ m/ground}}^2$ continued to decrease and reached a minimum at $D_p = \sim 50\text{ nm}$ ($r^2 = 0.18$), indicating the different sources at the two heights in this size range. The $\text{Ratio}_{260\text{ m/ground}}$ and $r_{260\text{ m/ground}}^2$ between 50 m and 300 nm increased monotonically with particle size, and reached peak values at $\sim 300\text{ nm}$ ($\text{Ratio}_{260\text{ m/ground}} = 0.75$, $r_{260\text{ m/ground}}^2 = 0.70$). This result suggested that the sources and concentrations of particles at the two heights became more similar as the increase of particle size. For particles larger than 300 nm, $\text{Ratio}_{260\text{ m/ground}}$ and $r_{260\text{ m/ground}}^2$ showed a small drop, while they remained relatively high. One explanation is that particles larger than 300 nm were relatively well mixed in a regional scale, although there were additional sources near ground.

Fig. 1d shows the correlation of size-resolved particle numbers between 260 m and ground level. The high correlations ($r_{260\text{ m/ground}}^2 > 0.4$) are located in particles larger than 100 nm, suggesting that these particles were more likely formed in a regional scale. The correlations between particles larger than 100 nm at 260 m and particles smaller than 100 nm at ground level were generally weak. Specifically, particles around 40 nm at ground level and particles around 50 nm at 260 m almost did not correlate with particles larger than 100 nm. These results indicating that the different sources, e.g. local emissions, contributed to particles smaller than 100 nm, especially for particles around 40 nm at ground level. We also noticed that particles in a nominal diameter at ground level correlated better with those in slightly larger sizes at 260 m, suggesting that particles could have grown to a larger size during vertical transport. Overall, we have a hypothesis that the increase of $\text{Ratio}_{260\text{ m/ground}}$ and $r_{260\text{ m/ground}}^2$ in Fig. 1c for particles smaller than 100 nm could be driven by the enhanced vertical mixing of local primary particles and secondary aerosols produced by local aging process, while regional transport plays a more important role for particles larger than 100 nm.

The temporal variations of PNSDs at 260 m and ground level from 21 November to 12 December are shown in Fig. 2. The vertical distribution of PNSD can be divided into 4 different types: 1) The number concentration of small size particles aloft was ubiquitously higher than that near ground ($\text{Ratio}_{260\text{ m/ground}} > 1.2$). This phenomenon mainly occurred in the first 3 clean days from 21 to 23 November (PM₁ was $7.2\ \mu\text{g m}^{-3}$ at 260 m and $10.7\ \mu\text{g m}^{-3}$ at ground level) under the conditions of northerly air mass and high wind speed above 5 m s^{-1} . Besides, the much higher concentration of O₃ (31 ppb at 260 m vs. 21 ppb at ground level) indicated a stronger photochemical processing at 260 m, associated with stronger NPF and growth events. 2) The number concentration of each size bin aloft was comparable to that near ground. This was mainly observed at noon caused by the enhanced mixing process, e.g., the period from 10:00 to 14:00 on 28 November. At the same time, the mass concentration of submicron aerosols was also comparable ($38.5\ \mu\text{g m}^{-3}$ at 260 m vs. $42.8\ \mu\text{g m}^{-3}$ at ground level) as well as concentrations of O₃, SO₂, and CO (Fig. S1). 3) The number concentration aloft was much lower than that near ground for small particles but slightly higher or comparable for large size particles. This mainly occurred at night on polluted days when the BL height was low but higher than 260 m. For instance, during the period from 20:00 on 2 December to 6:00 on 3 December, the average mass concentration was $128.4\ \mu\text{g m}^{-3}$ at 260 m and $134.8\ \mu\text{g m}^{-3}$ at ground level because of the comparable concentrations of large size particles ($D_p > 200\text{ nm}$, $\text{Ratio}_{260\text{ m/ground}} \geq 1$). However, low BL height ($305\text{ m} < \text{BLH} < 498\text{ m}$) resulted in the accumulation of local emissions so that the number concentration of small size particle was much higher near ground ($D_p < 200\text{ nm}$, $\text{Ratio}_{260\text{ m/ground}} < 0.5$). 4) The number concentration aloft was much lower than that near ground ($\text{Ratio}_{260\text{ m/ground}} < 0.5$). In this case, higher wind speed at 260 m and strong temperature inversions occurred frequently, and the boundary layer height was generally below 260 m. Thus, air pollutants at 260 m were scavenged quickly but remained high at ground level as observed on 4 December

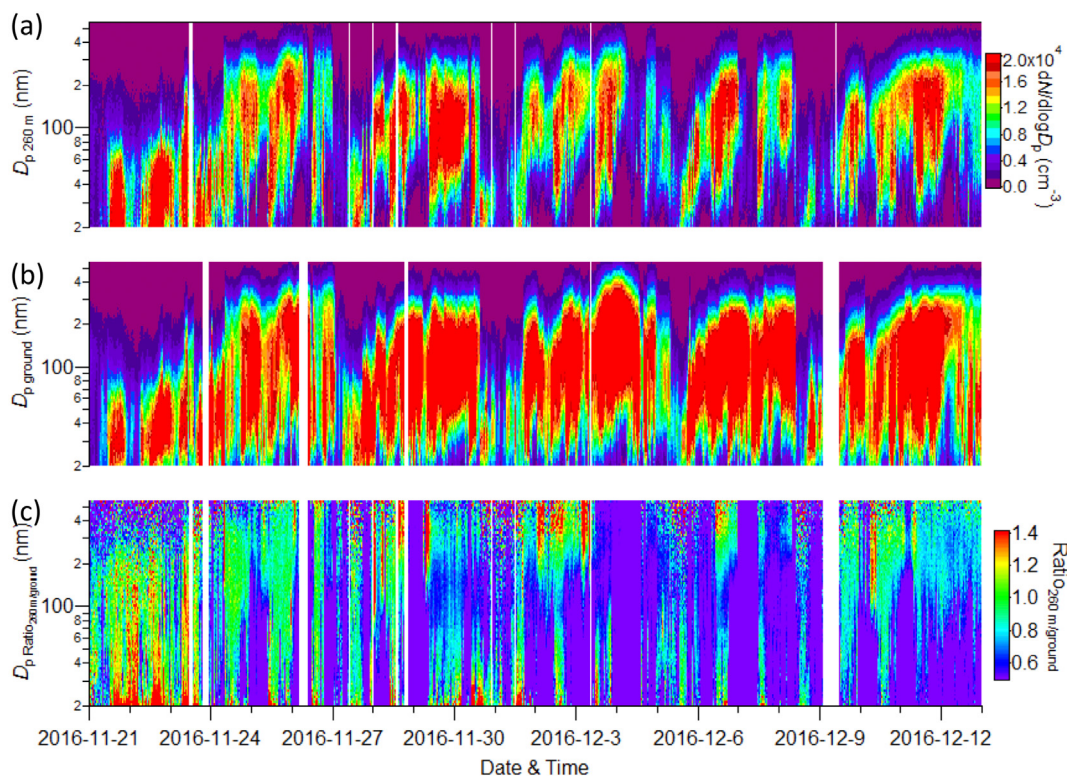


Fig. 2. Evolution of particle number size distributions at two heights. (a) and (b) show the time series of the particle number size distributions at 260 m and ground level, respectively. (c) Ratios of size-resolved particle number concentration at 260 m to that at ground level ($\text{Ratio}_{260\text{ m/ground}}$).

(175 m < BLH < 254 m). Huge differences of mass concentration and chemical composition between the two heights were also observed ($131.1 \mu\text{g m}^{-3}$ at 260 m vs. $321.4 \mu\text{g m}^{-3}$ at ground level).

3.2. Diurnal variations

The PNSD at ground level showed a pronounced diurnal variation (Fig. 3), showing 3 high concentration regions. A banana shape occurred after 17:00 with the geometric mean diameter (GMD) increased from ~40 nm to ~100 nm, indicating that the growth of locally emitted particles may also contribute to the accumulation mode particles under urban environment. During the growth process, the mass concentrations of all chemical species increased especially for organics (Fig. S6). Due to the dilution of particles without an immediate anthropogenic source, particle concentrations kept decreasing while the GMD remained stable after midnight.

As shown in Fig. 3a, the diurnal cycle of PNSD at 260 m was similar to that at ground level. However, there were significant differences indicated by the diurnal evolution of $\text{Ratio}_{260 \text{ m}/\text{ground}}$ and $r_{260 \text{ m}/\text{ground}}^2$. Both $\text{Ratio}_{260 \text{ m}/\text{ground}}$ and $r_{260 \text{ m}/\text{ground}}^2$ for particles smaller than 100 nm showed pronounced diurnal patterns, which had extremely low values at night time ($\text{Ratio}_{260 \text{ m}/\text{ground}} < 0.5$, $r_{260 \text{ m}/\text{ground}}^2 < 0.2$), indicating that these particles were strongly affected by vertical mixing processes associated with boundary layer dynamics.

Comparatively, larger particles had relatively higher ratios and correlation coefficients even at night time, especially for particles in the size range of 300–400 nm ($\text{Ratio}_{260 \text{ m}/\text{ground}} > 0.7$, $r_{260 \text{ m}/\text{ground}}^2 > 0.7$), suggesting these particles were well mixed in a regional scale. $\text{Ratio}_{260 \text{ m}/\text{ground}}$ and $r_{260 \text{ m}/\text{ground}}^2$ were close to 1 in all size bins especially between 12:00 and 16:00, suggesting similar PNSDs at different heights owing to strong vertical mixing under enhanced convective conditions. $\text{Ratio}_{260 \text{ m}/\text{ground}}$ beyond 1 was observed for particles smaller than 30 nm in the afternoon, suggesting a stronger source at 260 m. One of the possible explanations was the stronger NPF and growth at 260 m associated with stronger photochemical reaction, lower condensation sinks but higher vapor concentration (Fig. S6).

The diurnal cycles of particle number concentration in different size ranges at the two heights as well as their ratios and correlation coefficient are also illustrated in Fig. 3. The diurnal variation of N_{20-30} at ground level was characterized by a broad morning peak and a higher night peak. These peaks were mainly driven by traffic emissions (Section 3.4) and boundary layer height variation. However, the diurnal pattern of N_{20-30} at 260 m showed a broad high peak during daytime. It increased with N_{20-30} at ground level from 5:00 to 13:00 and $\text{Ratio}_{260 \text{ m}/\text{ground}}$ increased from ~0.30 to ~0.80. Since correlation coefficients were constantly low during this time, the source aloft was different from that near ground, and could be driven by NPF and growth events. N_{30-100} at both heights showed similar diurnal patterns,

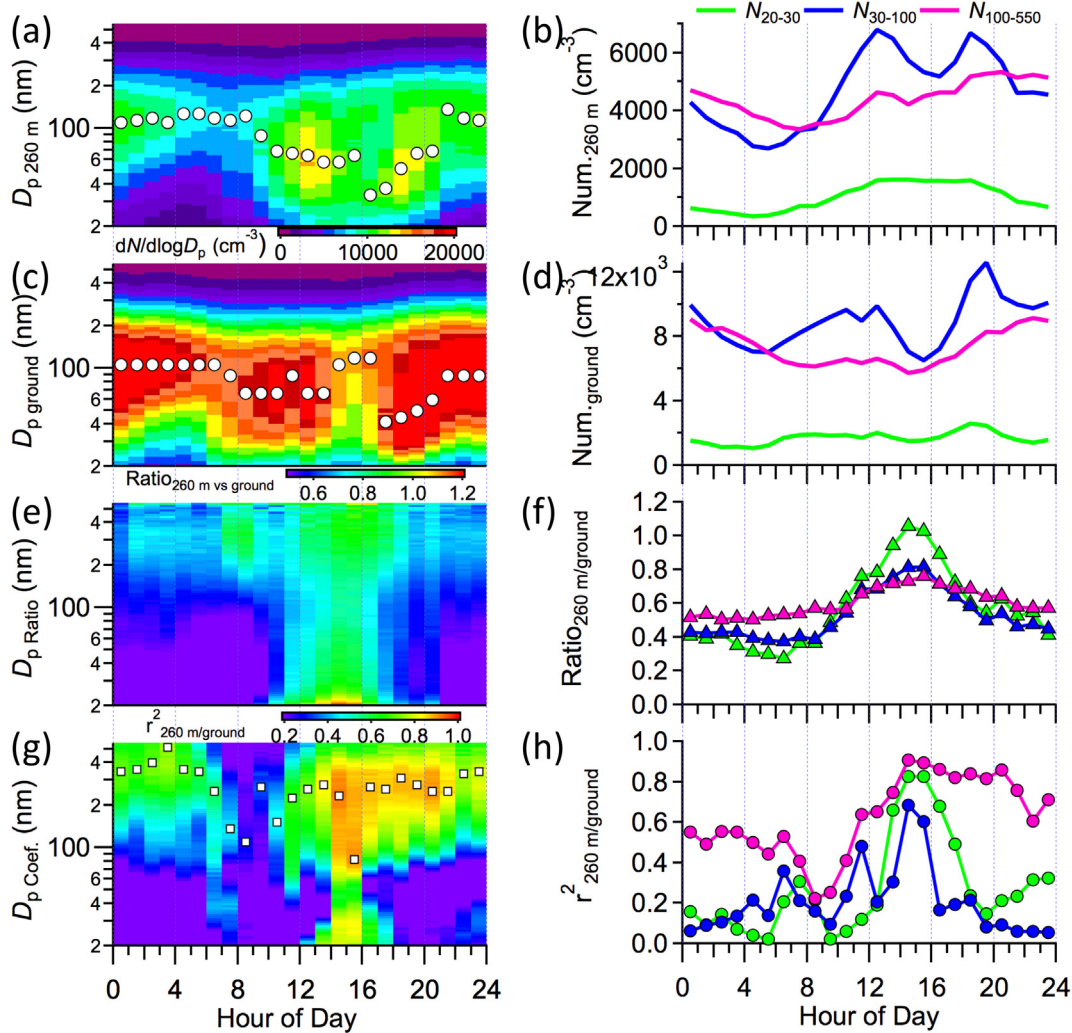


Fig. 3. Diurnal variations of particle number size distributions at two heights. Diurnal evolution of particle number size distribution (a) at 260 m, (c) at ground level, and (e) their ratios and (g) correlation coefficient. Diurnal variation of particle number concentration in different size range (b) at 260 m, (d) at ground level, and (f) their ratios and (h) correlation coefficient. White dots represent geometric mean diameter (GMD) in (a) and (c), and represent the best correlations in (g).

characterized by two high peaks. Note that N_{30-100} had a higher increasing rate at 260 m ($589 \text{ cm}^{-3} \text{ h}^{-1}$) than that at ground level ($411 \text{ cm}^{-3} \text{ h}^{-1}$) to reach the noon peak. Increasing correlation coefficients and ratios indicated that vertical mixing of local cooking emissions was enhanced associated with the rising BL height. On the contrary, the night peak of N_{30-100} was much higher at ground level ($12,581 \text{ cm}^{-3}$ at ground level vs. 6676 cm^{-3} at 260 m), which was mainly caused by the suppressed vertical transport. The diurnal evolution of accumulation mode particles ($N_{100-550}$) was smoother at both heights with slightly higher concentration at night. The ratios and correlations of $N_{100-550}$ between two heights were relatively stable at night time, indicating the dominant role of regional transport. $\text{Ratio}_{260 \text{ m}/\text{ground}}$ and $r_{260 \text{ m}/\text{ground}}^2$ of $N_{100-550}$ was higher during daytime, suggesting the vertical mixing also played a role.

3.3. Effect of meteorological parameters on the vertical distribution of PNSD

Fig. 4a shows the differences of wind vectors between two heights colored by $\text{Ratio}_{260 \text{ m}/\text{ground}}$. The wind direction followed the wind at 260 m, and the difference between the two heights was more significant when the dot was farther away from the origin. The total particle number concentration was totally different between two heights ($\text{Ratio}_{260 \text{ m}/\text{ground}} < 0.2$) when the wind at 260 m was from north, especially northwest, and the magnitude of wind difference was larger than 4 m s^{-1} . When the magnitude of wind difference was smaller than 4 m s^{-1} , $\text{Ratio}_{260 \text{ m}/\text{ground}}$ was generally high. Despite the large magnitude of wind difference, considerable total number concentrations contributed by abundant accumulation mode particles were observed when the winds came from south, especially southwest, coupled with relatively high $\text{Ratio}_{260 \text{ m}/\text{ground}}$ driven by regional transport (Fig. S7). The T differences ($\Delta T_{\text{ground}-260 \text{ m}}$) versus RH differences ($\Delta \text{RH}_{\text{ground}-260 \text{ m}}$) between two heights colored by $\text{Ratio}_{260 \text{ m}/\text{ground}}$ are illustrated in Fig. 4b. The smaller $\Delta T_{\text{ground}-260 \text{ m}}$ was always coupled with higher $\Delta \text{RH}_{\text{ground}-260 \text{ m}}$, indicating the weaker vertical mixing. $\text{Ratio}_{260 \text{ m}/\text{ground}}$ lower than 0.2 was mostly observed when $\Delta T_{\text{ground}-260 \text{ m}}$ was below 0 due to the occurrence of temperature inversion, which formed a stable atmosphere structure and suppressed the vertical mixing. Thus, one possible explanation for the large differences of particle numbers between 260 m and ground level was that the particles at 260 m were scavenged quickly by the high-speed wind from north, while the particles at ground level built up due to stable atmospheric structure, especially for N_{30-100} and $N_{100-550}$ (Fig. S7). It was also noted that N_{20-30} showed a different behaviour in the second wind quadrant, showing relative higher ratios and even

higher than 1. This result suggested the source of N_{20-30} particles aloft was different with that near ground, likely to be stronger new particle events. Our results illustrated that constant wind from north can clean-up haze pollution, while a sudden north wind increase the probability of inversion, which may have increased air pollution at ground level. The influences of temperature, RH on vertical differences of PNSDs between the two heights are then illustrated in more detail.

3.3.1. Temperature (T) effects

Fig. 5 shows the variations of PNSD as a function of temperature difference between ground level and 260 m ($\Delta T_{\text{ground}-260 \text{ m}}$). $\Delta T_{\text{ground}-260 \text{ m}} < 0$ indicates the presence of a temperature inversion. As the rising temperature inversion, the boundary layer height decreased obviously (Fig. S8), and the differences of PNSD between two heights were larger, confirmed by the decreased $\text{Ratio}_{260 \text{ m}/\text{ground}}$ and low $r_{260 \text{ m}/\text{ground}}^2$, highlighting the vertical mixing effects on vertical differences. Consistently, the number concentration was higher and particle size was larger at ground level, indicating that the presence of temperature inversion led to more severe haze at ground level. $\text{Ratio}_{260 \text{ m}/\text{ground}}$ for particles smaller than 100 nm was below 0.2 when $\Delta T_{\text{ground}-260 \text{ m}}$ was smaller than 1, due to the suppressed vertical mixing of local primary emissions at ground level. While large particles showed relatively high $\text{Ratio}_{260 \text{ m}/\text{ground}}$ with low $r_{260 \text{ m}/\text{ground}}^2$ within $\Delta T_{\text{ground}-260 \text{ m}}$ range from -3 to 1. The low $\text{Ratio}_{260 \text{ m}/\text{ground}}$ for large particles when $\Delta T_{\text{ground}-260 \text{ m}}$ was below -3 was a result of cleaning process aloft associated with the increased WS (Fig. S8). The ratios between two heights were close to 1 and even larger for small size particles when $\Delta T_{\text{ground}-260 \text{ m}} > 3$, which mainly occurred at noon time. One of the possible explanations was the stronger NPF at 260 m. Another reason was due to enhanced vertical mixing, which was supported by the high correlations and ratios in the size range of 60 to 200 nm. In general, $\text{Ratio}_{260 \text{ m}/\text{ground}}$ for total number concentration was a quadratic function of the differences of temperature ($\Delta T_{\text{ground}-260 \text{ m}}$) (Fig. S9). It showed that $\text{Ratio}_{260 \text{ m}/\text{ground}}$ increased with the increasing of $\Delta T_{\text{ground}-260 \text{ m}}$. When $\Delta T_{\text{ground}-260 \text{ m}}$ was above $2 \text{ }^\circ\text{C}$, $\text{Ratio}_{260 \text{ m}/\text{ground}}$ of total number larger than 1 was observed, mainly associated with high ratios of N_{20-30} (Fig. S9). This result supported the influence of NPF events due to low temperature at 260 m as well as the enhanced vertical transport due to large temperature difference.

Temperature inversion was frequently observed during our observation (Fig. S10), and 14 days with strong temperature inversions are listed in Table S1. They were further classified into 3 types: 1) Radiation inversion was mainly observed during clean periods. Because of temperature inversion, the transported particles aloft were difficult to

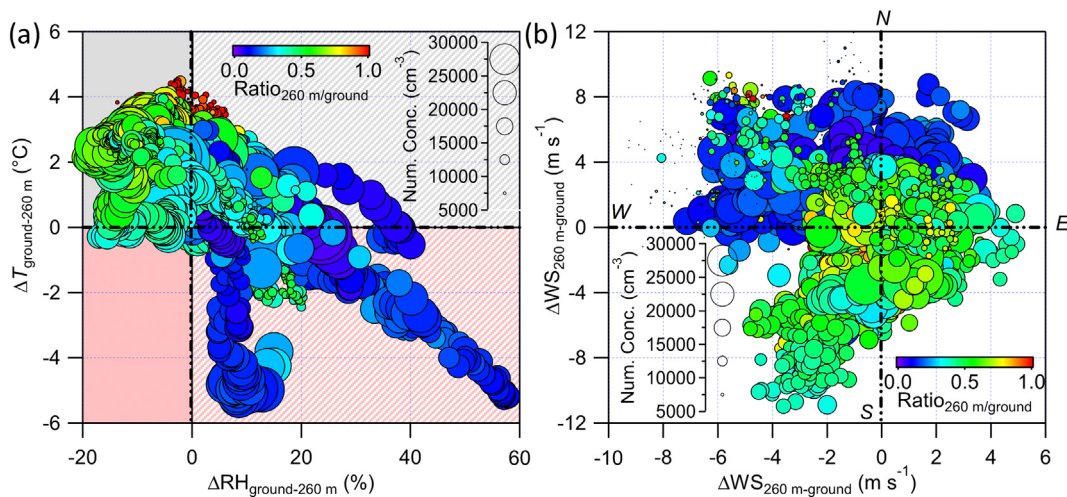


Fig. 4. Effect of meteorological parameters on the vertical distribution of total number concentration. (a) The differences of temperature ($\Delta T_{\text{ground}-260 \text{ m}}$) versus the differences of RH ($\Delta \text{RH}_{\text{ground}-260 \text{ m}}$) between ground level and 260 m. (b) The differences of wind vector between two heights, the marks N, W, S, E represent wind from north, west, south and east, respectively. The data are colored by the ratios of total number concentrations between two heights, and the marker size is proportional to the total number concentrations at ground level.

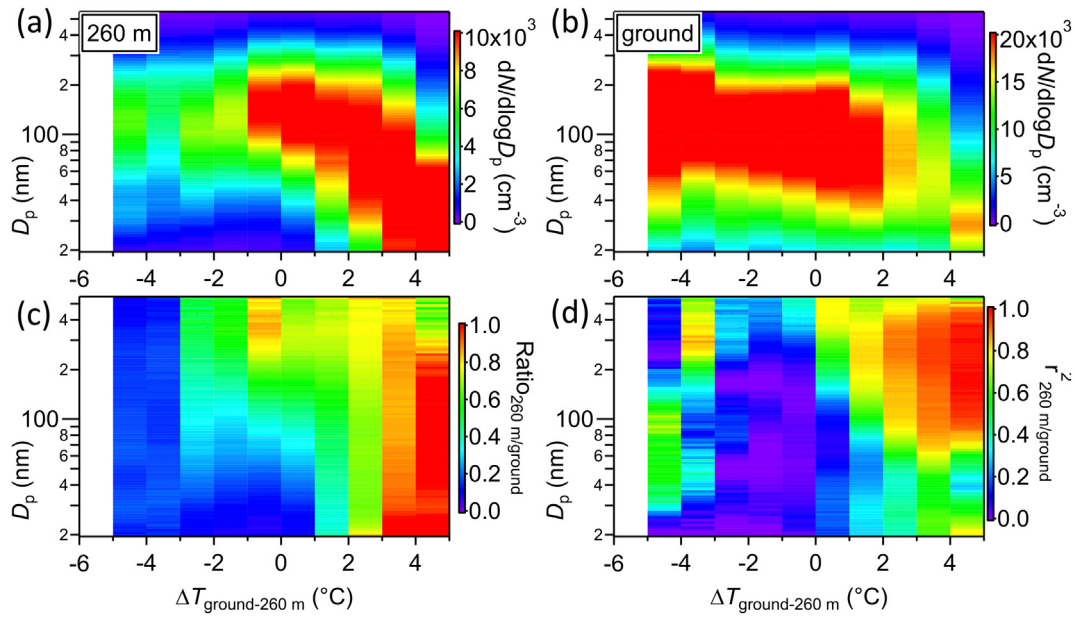


Fig. 5. Effect of temperature (T) on the vertical distribution of particle number size distributions. Particle number size distribution as a function of temperature difference ($\Delta T_{\text{ground-260 m}}$) at (a) 260 m and (b) ground level. (c) and (d) show the size-resolved ratios ($\text{Ratio}_{260 \text{ m/ground}}$) and correlation coefficient ($r_{260 \text{ m/ground}}^2$) between two heights, respectively.

reach the ground, which led to slightly higher mass concentration at 260 m associated with higher number concentration in the size range of 100–200 nm. Simultaneously, locally emitted particles at ground level were difficult to dilute as indicated by the higher number concentration for particles smaller than 100 nm at ground level, peaking at ~ 35 nm (Fig. S11a). 2) Frontal inversion associated with varying wind direction at different heights, was mainly observed during haze events. Frontal inversion was always formed along with a convergence zone near the surface layer and a divergence zone at high altitude. When the BL height was higher than 260 m, large particles showed similar distribution at both heights associated with the convergence of pollutants, while small particles were more abundant near ground because of the extremely unfavourable conditions for locally emitted pollutants to diffuse, e.g. 3 December (Fig. S11b). When the boundary layer was lower than 260 m, PNSD at 260 m were completely different in all size bins, e.g. 30 November. 3) Foehn inversion was mainly observed during haze clean-up period. Defined as warm, dry wind descending in the lee of a mountain range, foehn wind was frequently observed at the eastern foot of Taihang (Wang et al., 2012). In this study, the inversion occurred when the warm and extremely dry ($\text{RH} < 20\%$) air from the northwest at a high speed heated the temperature at 260 m before sunrise, e.g., 7 December. In this case, particles at ground level showed high concentration dominated by particles larger than 100 nm. However, pollutants were cleaned up quickly at high altitude, which led to the extremely low number concentration at 260 m. Despite the vast difference in number concentration, PNSDs at both heights showed similar bimodal size distribution profiles, peaking at ~ 30 nm and ~ 100 nm, respectively (Fig. S11c).

3.3.2. Relative humidity (RH) effects

Fig. 6 shows the variations of PNSD as a function of RH at 260 m and ground level. The data with $\Delta \text{RH}_{\text{ground-260 m}} > 13$ were excluded to better characterize the RH effects on vertical distributions (Fig. S12). At ground level (Fig. 6b), the influence of RH on particle number concentrations depended on particle size. Small particles showed high concentrations at low RH while large particles, showed high concentrations at high RH. The geometric mean diameters were 37.2 nm and 140.7 nm at 10% and at 90%, respectively, suggesting that particles shifted towards larger size at higher RH levels. The evolution of the total number concentration as a function of RH can be divided into three stages. 1) The

total number concentration increased at a considerable rate ($3856 \text{ cm}^{-3}/10\% \text{ RH}$) during the first stage ($\text{RH} < 50\%$). Such a change was mainly driven by the increase of N_{30-100} ($1351 \text{ cm}^{-3}/10\% \text{ RH}$) and $N_{100-550}$ ($2638 \text{ cm}^{-3}/10\% \text{ RH}$), while the N_{20-30} stayed relatively stable. As a result, the number fraction of $N_{100-550}$ increased from 13% to 42% associated with the decreases in N_{20-30} from 24% to 9%. During this growth process, all chemical species increased in mass concentrations, mostly organics and nitrate (Fig. S13). Organics increased from 6.0 to $44.6 \mu\text{g m}^{-3}$ although the mass fraction decreased by 12%, while NO_3 increased from 0.8 to $19.8 \mu\text{g m}^{-3}$, with an increase of mass fraction by 8%. 2) During the second stage ($\text{RH} = 50\text{--}70\%$), the total particle number concentration remained relatively stable, while the particle mass showed a much stronger increasing trend than that in stage 1. Consistently, accumulation mode particles increased from 9153 to $11,688 \text{ cm}^{-3}$ associated with the decrease in N_{20-30} particles. This phenomenon was more pronounced at night, indicating that high RH facilitated the growth of particle size because of enhanced heterogeneous reaction. This is further supported by the increased fraction of sulfate during this stage. 3) After that, the total number concentration and $N_{100-550}$ increased as RH increased from 70% to 90%, mainly at night time.

Although a similar pattern was observed at 260 m, significant differences were also observed. 1) The total number concentration showed a continuously increasing trend between 10% and 70%, mainly due to the increases in N_{30-100} and $N_{100-550}$. The increasing rate was $2327 \text{ cm}^{-3}/10\%$ from 10% and 40%, which was lower than that at ground level. Different from that at ground level, the increasing trend was more pronounced during daytime, indicating the influences of NPF and photochemical reaction. The high correlation between two heights during daytime ($r_{260 \text{ m/ground}}^2 > 0.7$) suggested that the effects of vertical mixing were also important. Organics and nitrate seemed to play important roles at 260 m as well. Between 40% and 70%, a lower increasing rate of total number concentration was observed ($1023 \text{ cm}^{-3}/10\% \text{ RH}$). The increased correlation between the two heights indicated that it was mainly caused by the enhanced vertical transport of ground particles, which led to the decrease in GMD. 2) Above 70%, the total number concentration began to decrease while the particle mass remained relatively stable. Considering the increase of GMD, coagulation growth was likely to be important because of the increase in particle viscosity under high RH levels.

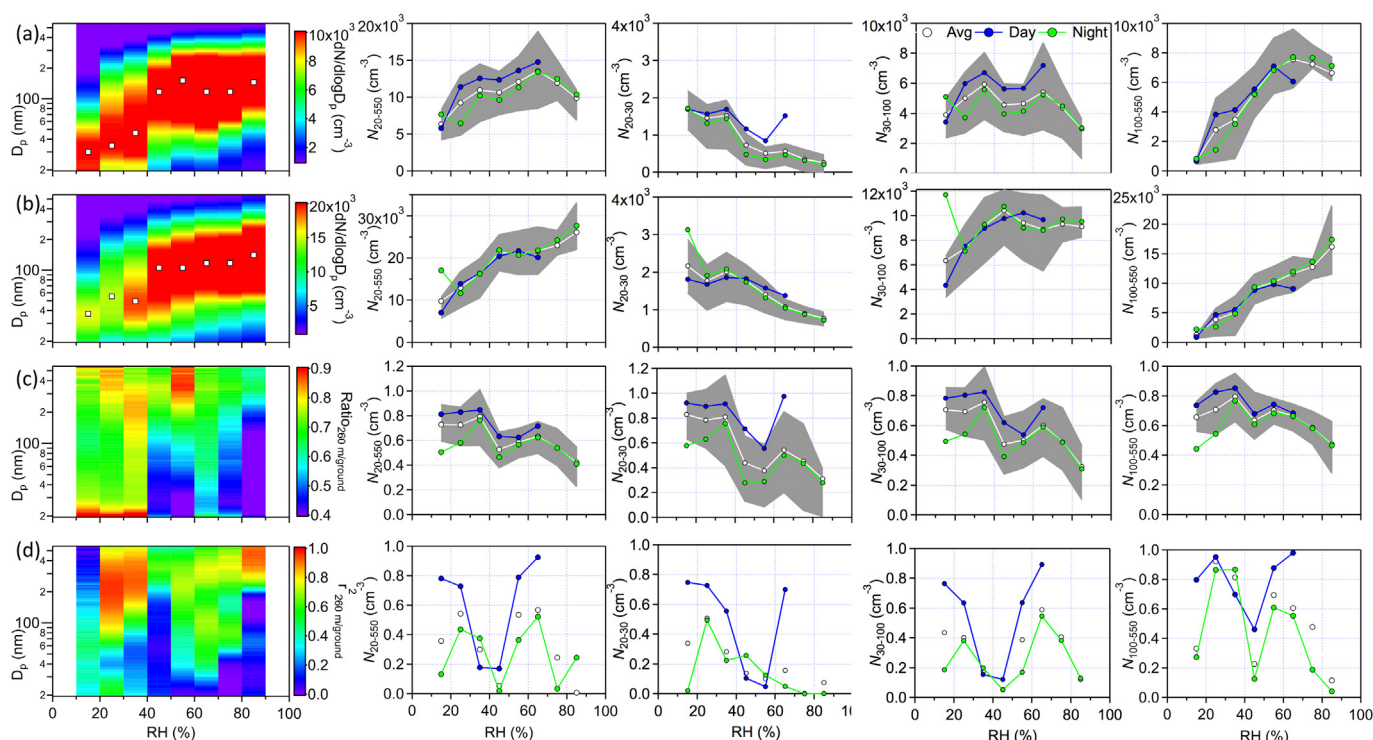


Fig. 6. Effect of relative humidity (RH) on the vertical distribution of particle number size distributions. Variations of size-resolved number concentration at (a) 260 m and (b) ground level, (c) their ratios ($\text{Ratio}_{260 \text{ m/ground}}$) and (d) correlation coefficients ($r^2_{260 \text{ m/ground}}$) as a function of RH, respectively. The data are grouped in RH bins (10% increment), and the shaded areas indicate the 25th and 75th percentiles.

The evolution of size-resolved ratios of number concentration between the two heights as a function of RH showed that smaller particles had higher $\text{Ratio}_{260 \text{ m/ground}}$ when the RH was low while $\text{Ratio}_{260 \text{ m/ground}}$ of large size particles remained relatively stable as the evolution of RH, especially for particles around 300 nm. In general, $\text{Ratio}_{260 \text{ m/ground}}$ of total number concentration and those in three modes showed similar downward trends as the increasing of RH (RH < 90%). This suggests that the higher RH led to a larger vertical difference between the two heights. One possible reason was that heterogeneous reactions were more pronounced under relatively high RH levels (>50%) at ground level because of the additional local source emissions. Another reason was that higher RH was generally associated with stagnant meteorological conditions when the vertical mixing was weak.

3.4. Source apportionment

PMF analysis of PNSD resolved six factors in winter in Beijing. Corresponding to NPF and growth events in Fig. 1, the time series of number concentration of factor 1 in Fig. 7c was characterized by sharp peaks on clean days. Since the nucleation mode particles were smaller than 20 nm (Kulmala et al., 2004), the size distribution of factor 1 showed incomplete patterns at both heights, seeming to peak under 20 nm. Similar PNSD was attributed to nucleation mode particles from the dilution of vehicle exhaust emission (Liu et al., 2014). Casati et al. (2007) found that the emission rate of nucleation mode particles peaking under 20 nm during the dilution of vehicle exhaust is higher at low temperatures. Thus, factor 1 at ground level was reported as a complex factor, which was dominated by the dilution of vehicle exhaust emission as well as the influence of NPF events during daytime in clean days. This speculation was consistent with the diurnal evolution at ground level, which showed three high peaks associated with traffic emission and NPF events (Fig. 8). Comparatively, the time series of factor 1 at 260 m was more pronounced, and the diurnal pattern at 260 m showed a rapid increase from 87 cm^{-3} at 6:00 to 612 cm^{-3} at 14:00, suggesting the dominant source of NPF rather than traffic emissions.

Consistently, $\text{Ratio}_{260 \text{ m/ground}}$ increased from 0.5 to 2.0, due to stronger NPF events associated with higher SO_2 and O_3 concentration but relatively lower condensation sink.

With relatively high correlation with factor 1 ($r^2 = 0.65$ at 260 m vs. $r^2 = 0.59$ at ground level), the temporal variations of factor 2 were likely to echo high peaks in factor 1 at both heights. The profile of factor 2 peaked at around 30 nm, dominated by ultrafine particles in the size range from 20 to 50 nm. This profile at ground level was similar to the traffic emission found in previous studies (Gu et al., 2011; Kim et al., 2004; Ogulei et al., 2007; Sowlat et al., 2016; Zhou, 2005). The diurnal evolution of number concentration and fraction of factor 2 at ground level showed two pronounced peaks, i.e. in the early morning (8:00) and evening (19:00) associated with traffic rush hours. Therefore, factor 2 at ground level was a mixed factor with the contributions from both traffic emissions and particle growth, yet they cannot be separated due to similar PNSD. Although it showed comparable proportion at both heights, factor 2 had lower concentration aloft (1359 cm^{-3}) than that near ground (2595 cm^{-3}). Similar to factor 1 at 260 m, the particle number concentrations of factor 2 at 260 m started to increase from 435 cm^{-3} at 6:00, and then remained relatively high concentrations until reaching 2253 cm^{-3} at 19:00. Correspondingly, the number fraction of factor 2 at 260 m increased to 20% at 19:00. The high correlations ($r^2_{260 \text{ m/ground}} > 0.8$) in the late afternoon suggested that vertical transport from ground level also contribute to factor 2 at 260 m. However, the overall correlation of factor 2 between two heights was relatively low (0.31), indicating that the sources were not the same. This result supported that factor 2 at 260 m mainly represented the growth of newly formed particles while that near ground was more contributed by traffic emissions.

Factor 3 was dominated by the Aitken mode particles peaking at around 50 nm, which was in agreement with PNSDs for cooking activities (Buonanno et al., 2011; Géhin et al., 2008). Consistently, the time series of factor 3 was only related to COA, although the correlation coefficient was not high due to the lower detection efficiency of AMS at small size particles (Fig. S14). Accounting for 26% (an average of

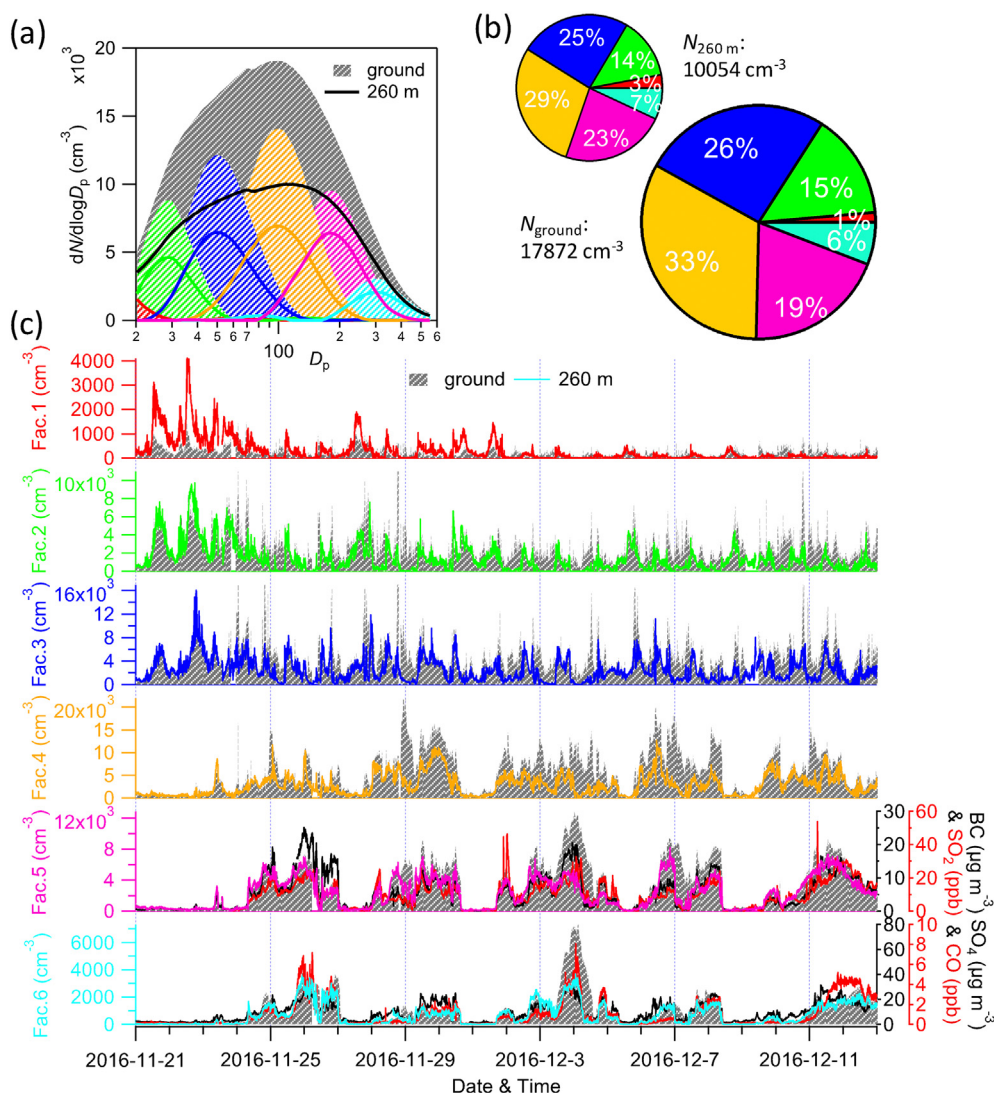


Fig. 7. Particle sources identified by positive matrix factorization. (a) Factor profiles of size-resolved particle number concentration at 260 m and ground level via PMF analysis. (b) Average contribution of 6 PMF factors at 260 m and ground level. (c) Time series of PMF factors at ground level and 260 m.

4657 cm⁻³), the number concentration of this factor at ground level had sharp peaks almost every day and showed a pronounced diurnal pattern with two peaks (12:00–13:00 vs. 19:00–20:00) associated with cooking activities. The much higher peak (~7997 cm⁻³) in the evening could be explained by the cooking emissions significantly enhanced at night time and the shallow boundary layer in winter in Beijing. Such a diurnal profile was consistent with the resolved cooking emissions reported by Du et al. (2017), and also remarkably similar to that of cooking organic aerosol which was widely reported in Beijing (Elser et al., 2016; X.F. Huang et al., 2010; Sun et al., 2013; Xu et al., 2015; Zhang et al., 2016; Zhao et al., 2017). Hence, factor 3 at ground level was related to primary cooking emissions. At 260 m, factor 3 had a similar fraction with that at ground level, accounting for 25%. However, the average number concentration of factor 3 aloft was 2481 cm⁻³, which was 47% lower than that near ground (4657 cm⁻³). The time series of factor 3 at 260 m tracked well with that at ground level, and the diurnal profile of factor 3 aloft was also similar to that near ground but much smoother. At night time, the vertical transport of local emission from ground to high altitude was suppressed by the increased atmospheric stability, leading to larger differences ($\text{Ratio}_{260\text{ m}/\text{ground}} = 0.4$) and low correlation ($r_{260\text{ m}/\text{ground}}^2 = 0.2$). Thus, the night peak aloft was much lower than that near ground. These results suggested that factor 3 at

260 m were mainly contributed by cooking emitted particles transported from ground level.

Peaking at around 100 nm, factor 4 was mostly represented by particles in the size range of 50–200 nm at both heights. With an average of 5851 cm⁻³, this factor at ground level dominated total number concentration (33%). The temporal variations showed high concentration levels during haze pollution. Compared to the other 5 factors, factor 4 had the highest correlation with O₃, and it was also found to be associated with primary emissions, e.g. SO₂, CO, BC, and POA factors (Fig. S14). These results suggested that this factor at ground level was associated with aging process. The diurnal variation of factor 4 near ground was similar to that of OPOA, which was characterized by high concentrations during night and a small noon peak. The average concentration of factor 4 aloft was 2880 cm⁻³, which was 52% lower than that near ground. Contributing 29% on average to the total number concentration, the number fraction of this factor at 260 m varied between 21% and 37%. The time series of factor 4 tracked relatively well at two heights ($r^2 = 0.46$), and the diurnal evolution at 260 m had the same trend with that at ground level. The increasing rate during daytime at 260 m (310 cm⁻³ h⁻¹) was twice faster than that at ground level (154 cm⁻³ h⁻¹), leading to an increase in $\text{Ratio}_{260\text{ m}/\text{ground}}$ from 0.4 to 0.6, likely indicating the enhanced aging process at 260 m due to

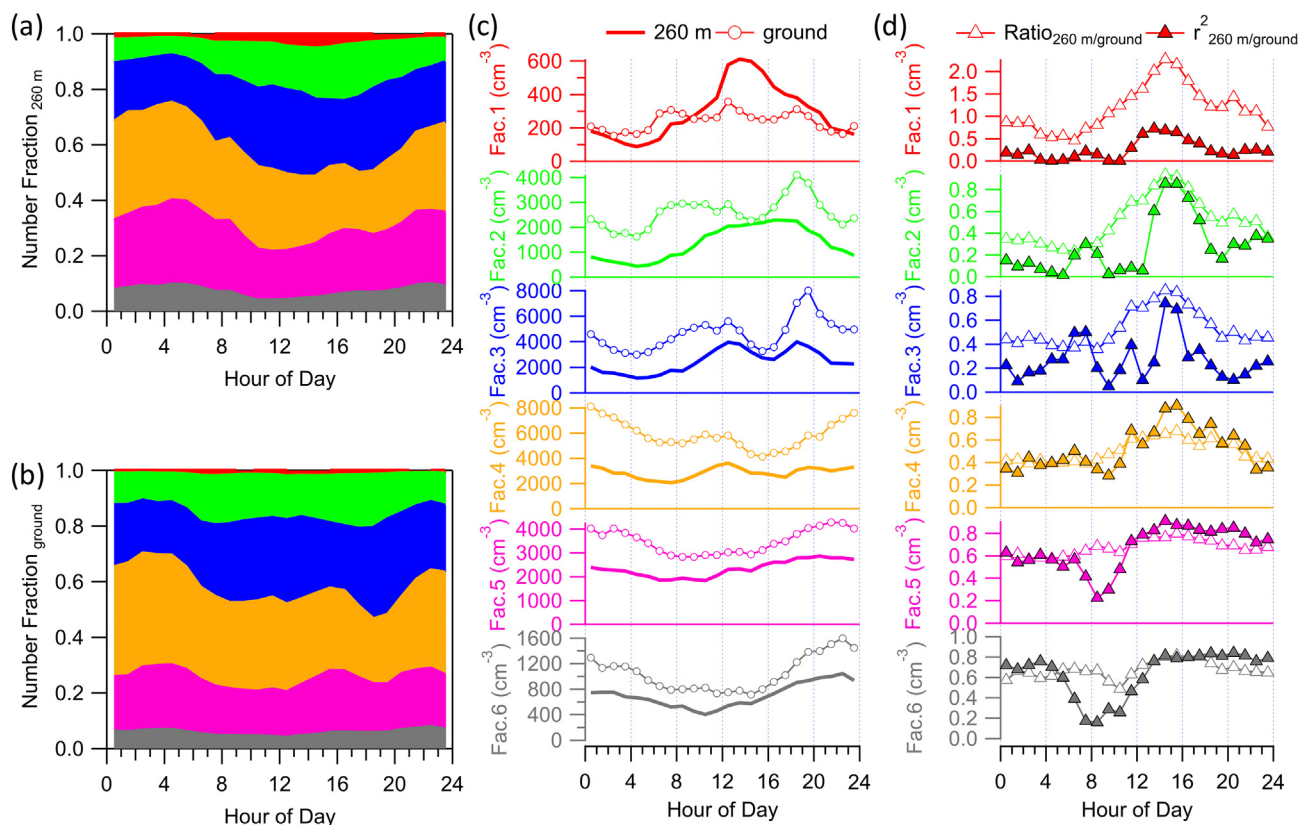


Fig. 8. Diurnal variations of particle sources. Average diurnal variations of number fraction of PMF factors at (a) ground level and (b) 260 m. (c) shows a comparison of the average diurnal cycles of particle number concentrations for PMF factors at ground level and 260 m. (d) shows the diurnal cycles of ratios and correlations between 260 m and the ground level for PMF factors.

stronger photochemical reaction aloft. However, low $\text{Ratio}_{260\text{ m}/\text{ground}}$ at night time with low $r_{260\text{ m}/\text{ground}}^2$ was also observed, suggesting the aging process was suppressed at 260 m because less gaseous precursors were transported from ground due to more stable boundary layer at night time.

Accounting for 23% aloft and 19% at ground level, the PNSD of factor 5 peaked at around 180 nm, similar to that from residential heating Ogulei et al. (2007). The average number concentration of this factor was 3483 cm^{-3} at ground level, which was 49% higher than that at 260 m (2337 cm^{-3}). The temporal variations correlated well between two heights ($r^2 = 0.67$), and also correlated well with species indicative of combustion emissions, e.g. SO_2 ($r^2 = 0.58$ aloft vs. $r^2 = 0.60$ near ground), CO ($r^2 = 0.72$ aloft vs. $r^2 = 0.79$ near ground), BC ($r^2 = 0.69$ aloft vs. $r^2 = 0.82$ near ground), and BBOA ($r^2 = 0.74$ near ground) (Fig. S14). The diurnal cycle of number concentration was characterized by high levels at night and low values during daytime, which was in agreement with BBOA, and coal combustion organic aerosols resolved in Beijing (Sun et al., 2013; Wang et al., 2015). The $\text{Ratio}_{260\text{ m}/\text{ground}}$ was relatively stable (0.6–0.8) throughout the day, and the $r_{260\text{ m}/\text{ground}}^2$ was also high except early morning, indicating that aerosol particles in this factor were relatively well mixed in a regional scale.

Factor 6 was identified as a regional secondary aerosol. With a similar contribution at both heights (6% at ground level vs. 7% at 260 m), this factor was dominated by a particle mode at around 300 nm, which was suggested as secondary aerosols over a regional scale in previous studies (Du et al., 2017; Gu et al., 2011; Liu et al., 2016; Wang et al., 2013). The temporal variations were highly correlated between two heights ($r^2 = 0.67$), and also correlated with secondary inorganic aerosols including sulfate ($r^2 = 0.77$ aloft and $r^2 = 0.83$ near ground) and nitrate ($r^2 = 0.84$ aloft and $r^2 = 0.83$ near ground), suggesting that these particles are formed over a regional scale that had been relatively well aged in the atmosphere (Fig. S14). Consistently, compared to other

factors, factor 6 at ground level showed the highest correlation with SOA factors identified by PMF. The diurnal variation of number concentration and fraction of this factor was much smoother and showed consistently high concentration during nighttime at both heights, which was consistent with previously reported regional aerosols (Liu et al., 2016). In fact, the correlation coefficients between two heights were always larger than ~ 0.7 , except for the small decrease in the early morning associated with the different WS and WD at different heights (Fig. S6).

Overall, the PNSD at 260 m dominated by secondary aerosols (52%), i.e., factors 1, 2, 4, and 6, was more representative over a regional scale, while that at ground level was more influenced by primary emissions (60%), i.e., factors 2, 3 and 5 especially traffic and cooking emissions. Secondary aerosols that were formed from local production, i.e., factor 4, dominated the total number concentration at both heights (29% aloft vs. 33% near ground), while the number concentration of secondary aerosols formed over a regional scale, i.e., factor 6, was comparably low (7% aloft vs. 6% near ground). However, factor 6 accounted for nearly half of the total volume concentration (46% aloft vs. 44% near ground) highlighting that local emissions and regional transport contributed significantly differently to the number and mass concentrations (Fig. S15).

4. Conclusions

PNSDs were measured simultaneously at ground level and at 260 m in urban Beijing from 21 November to 13 December 2016. Our study shows significant differences in PNSDs between the two heights in winter. The average number concentration near ground ($17,878\text{ cm}^{-3}$) was 78% higher than that aloft ($10,065\text{ cm}^{-3}$). The ratios of PNSD between the two heights depended strongly on particle size and changed dramatically throughout the observation, resulting from the complex interaction between boundary layer dynamics, meteorological conditions,

particle sources, and processes. Particles larger than 200 nm were mainly formed over a regional scale and relatively well-mixed, and thus had smaller differences ($\text{Ratio}_{260\text{ m/ground}} = 0.75$ at 300 nm) with tight correlations ($r_{260\text{ m/ground}}^2 = 0.70$ at 300 nm) between ground level and urban aloft. Particles in the size range from 30 to 100 nm were dominated by local emitted particles associated with traffic and cooking activities, and thus showed a pronounced diurnal evolution of $\text{Ratio}_{260\text{ m/ground}}$ with high values in the afternoon because of the enhanced vertical mixing due to high BL height. Particles smaller than 30 nm were mainly attributed to new particle formation and growth events at 260 m, while they were more affected by traffic emissions at ground level, leading to higher $\text{Ratio}_{260\text{ m/ground}}$ than unit during noontime. Meteorological conditions (e.g., winds, RH, and T) also played important roles in driving the vertical differences in PNSD. The vertical ratios decreased as the temperature difference of the two heights was small and the atmospheric boundary layer was stable. Particularly, we found that the arrival of northerly winds increased the probability of temperature inversion and worsened air pollution at ground level during early period although it cleaned up particles at high altitude first.

Data availability

The data in this study are available from the authors upon request (sunyele@mail.iap.ac.cn).

Funding

This work was supported by the National Natural Science Foundation of China (91744207, 92044301), Academy of Finland via Center of Excellence in Atmospheric Sciences (project no. 272041) and European Research Council via ATM-GTP 266 (742206). This research has also received funding from Jane and Aatos Erkkö Foundation and Academy of Finland Flagship funding (grant no. 337549).

CRedit authorship contribution statement

WD and YS conceived the study. WD, WW, YW, YZ, JZ, CX, QW, WX, WZ, FZ, ZL, PF, JL, MG conducted the field measurements. WD, JZ, WX carried out the data analysis. RL, LD, JK, ZW, MK, YS participated in the discussions. MK, YS supported this research. WD wrote the paper with inputs from all co-authors.

Declaration of competing interest

The authors declare that they have no known competing financial interests or personal relationships that could have appeared to influence the work reported in this paper.

Appendix A. Supplementary data

Supplementary data to this article can be found online at <https://doi.org/10.1016/j.scitotenv.2021.149695>.

References

- Buonanno, G., Johnson, G., Morawska, L., Stabile, L., 2011. Volatility characterization of cooking-generated aerosol particles. *Aerosol Sci. Technol.* 45, 1069–1077.
- Cai, J., Chu, B., Yao, L., Yan, C., Heikkinen, L.M., Zheng, F., Li, C., Fan, X., Zhang, S., Yang, D., Wang, Y., Kokkonen, T.V., Chan, T., Zhou, Y., Dada, L., Liu, Y., He, H., Paasonen, P., Kujansuu, J.T., Petäjä, T., Mohr, C., Kangasluoma, J., Bianchi, F., Sun, Y., Croteau, P.L., Worsnop, D.R., Kerminen, V.-M., Du, W., Kulmala, M., Daellenbach, K.R., 2020. Size-segregated particle number and mass concentrations from different emission sources in urban Beijing. *Atmos. Chem. Phys.* 20, 12721–12740.
- Casati, R., Scheer, V., Vogt, R., Benter, T., 2007. Measurement of nucleation and soot mode particle emission from a diesel passenger car in real world and laboratory in situ dilution. *Atmos. Environ.* 41, 2125–2135.
- Du, W., Dada, L., Zhao, J., Chen, X., Daellenbach, K.R., Xie, C., Wang, W., He, Y., Cai, J., Yao, L., Zhang, Y., Wang, Q., Xu, W., Wang, Y., Tang, G., Cheng, X., Kokkonen, T.V., Zhou, W., Yan, C., Chu, B., Zha, Q., Hakala, S., Kurppa, M., Järvi, L., Liu, Y., Li, Z., Ge, M., Fu, P.,

- Nie, W., Bianchi, F., Petäjä, T., Paasonen, P., Wang, Z., Worsnop, D.R., Kerminen, V.-M., Kulmala, M., Sun, Y., 2021. A 3D study on the amplification of regional haze and particle growth by local emissions. *npj Clim. Atmos. Sci.* 4, 4.
- Du, W., Zhao, J., Wang, Y., Zhang, Y., Wang, Q., Xu, W., Chen, C., Han, T., Zhang, F., Li, Z., Fu, P., Li, J., Wang, Z., Sun, Y., 2017. Simultaneous measurements of particle number size distributions at ground level and 260 m on a meteorological tower in urban Beijing, China. *Atmos. Chem. Phys.* 17, 6797–6811.
- Dusek, U., Frank, G.P., Hildebrandt, L., Curtius, J., Schneider, J., Walter, S., Chand, D., Drewnick, F., Hings, S., Jung, D., Borrmann, S., Andreae, M.O., 2006. Size matters more than chemistry for cloud-nucleating ability of aerosol particles. *Science* 312, 1375–1378.
- Elser, M., Huang, R.-J., Wolf, R., Slowik, J.G., Wang, Q., Canonaco, F., Li, G., Bozzetti, C., Daellenbach, K.R., Huang, Y., Zhang, R., Li, Z., Cao, J., Baltensperger, U., El-Haddad, I., Prévôt, A.S.H., 2016. New insights into PM_{2.5} chemical composition and sources in two major cities in China during extreme haze events using aerosol mass spectrometry. *Atmos. Chem. Phys.* 16, 3207–3225.
- Gao, J., Chai, F., Wang, T., Wang, S., Wang, W., 2012. Particle number size distribution and new particle formation: new characteristics during the special pollution control period in Beijing. *J. Environ. Sci.* 24, 14–21.
- Géhin, E., Ramalho, O., Kirchner, S., 2008. Size distribution and emission rate measurement of fine and ultrafine particle from indoor human activities. *Atmos. Environ.* 42, 8341–8352.
- Gu, J., Pitz, M., Schnelle-Kreis, J., Diemer, J., Reller, A., Zimmermann, R., Soentgen, J., Stoelzel, M., Wichmann, H.E., Peters, A., Cyrys, J., 2011. Source apportionment of ambient particles: comparison of positive matrix factorization analysis applied to particle size distribution and chemical composition data. *Atmos. Environ.* 45, 1849–1857.
- Guo, S., Hu, M., Zamora, M.L., Peng, J., Shang, D., Zheng, J., Du, Z., Wu, Z., Shao, M., Zeng, L., Molina, M.J., Zhang, R., 2014. Elucidating severe urban haze formation in China. *Proc. Natl. Acad. Sci. USA* 111, 17373–17378.
- Huang, S., Liu, J., Liu, W., Lu, Y., Lu, F., Wu, D., Dong, Y., Jiang, Y., Zhang, Y., 2010a. Influence of high humidity in summer on the characteristic of Aerosol's size distribution in Beijing. *J. Environ. Sci. (China)* 31, 17–21.
- Huang, X.F., He, L.Y., Hu, M., Canagaratna, M.R., Sun, Y., Zhang, Q., Zhu, T., Xue, L., Zeng, L.W., Liu, X.G., Zhang, Y.H., Jayne, J.T., Ng, N.L., Worsnop, D.R., 2010b. Highly time-resolved chemical characterization of atmospheric submicron particles during 2008 Beijing olympic games using an aerodyne high-resolution aerosol mass spectrometer. *Atmos. Chem. Phys.* 10, 8933–8945.
- Kim, E., Hopke, P.K., Larson, T.V., Covert, D.S., 2004. Analysis of ambient particle size distributions using unmix and positive matrix factorization. *Environ. Sci. Technol.* 38, 202–209.
- Kulmala, M., Dada, L., Daellenbach, K.R., Yan, C., Stolzenburg, D., Kontkanen, J., Ezhova, E., Hakala, S., Tuovinen, S., Kokkonen, T.V., 2021. Is reducing new particle formation a plausible solution to mitigate particulate air pollution in Beijing and other Chinese megacities? *Faraday Discuss.* 226, 334–347.
- Kulmala, M., Vehkamäki, H., Petäjä, T., Dal Maso, M., Lauri, A., Kerminen, V.M., Birmili, W., McMurry, P.H., 2004. Formation and growth rates of ultrafine atmospheric particles: a review of observations. *J. Aerosol Sci.* 35, 143–176.
- Lang, F., Yan, W., Zhang, Q., Cao, J., 2013. Size distribution of atmospheric particle number in Beijing and association with meteorological conditions. *China Environ. Sci.* 33, 1153–1159.
- Liu, Z., Wang, Y., Hu, B., Ji, D., Zhang, J., Wu, F., Wan, X., Wang, Y., 2016. Source appointment of fine particle number and volume concentration during severe haze pollution in Beijing in January 2013. *Environ. Sci. Pollut. Res.* 23, 6845–6860.
- Liu, Z.R., Hu, B., Liu, Q., Sun, Y., Wang, Y.S., 2014. Source apportionment of urban fine particle number concentration during summertime in Beijing. *Atmos. Environ.* 96, 359–369.
- Ogulei, D., Hopke, P.K., Chalupa, D.C., Utell, M.J., 2007. Modeling source contributions to submicron particle number concentrations measured in Rochester, New York. *Aerosol Sci. Tech.* 41, 179–201.
- Olivares, G., Johansson, C., Ström, J., Hansson, H.-C., 2007. The role of ambient temperature for particle number concentrations in a street canyon. *Atmos. Environ.* 41, 2145–2155.
- Paatero, P., Tapper, U., 1994. Positive matrix factorization - a nonnegative factor model with optimal utilization of error-estimates of data values. *Environmetrics* 5, 111–126.
- Peng, J.F., Hu, M., Wang, Z.B., Huang, X.F., Kumar, P., Wu, Z.J., Guo, S., Yue, D.L., Shang, D.J., Zheng, Z., He, L.Y., 2014. Submicron aerosols at thirteen diversified sites in China: size distribution, new particle formation and corresponding contribution to cloud condensation nuclei production. *Atmos. Chem. Phys.* 14, 10249–10265.
- Seaton, A., Macnee, W., Donaldson, K., Godden, D., 1995. Particulate air-pollution and acute health-effects. *Lancet* 345, 176–178.
- Seinfeld, J.H., Pandis, S.N., 2016. *Atmospheric Chemistry and Physics: From Air Pollution to Climate Change*. John Wiley & Sons.
- Shen, X.J., Sun, J.Y., Zhang, X.Y., Zhang, Y.M., Zhang, L., Fan, R.X., Zhang, Z.X., Zhang, X.L., Zhou, H.G., Zhou, L.Y., Dong, F., Shi, Q.F., 2016. The influence of emission control on particle number size distribution and new particle formation during China's V-day parade in 2015. *Sci. Total Environ.* 573, 409–419.
- Sowlat, M.H., Hasheminassab, S., Sioutas, C., 2016. Source apportionment of ambient particle number concentrations in Central Los Angeles using positive matrix factorization (PMF). *Atmos. Chem. Phys. Discuss.* 1–42.
- Sun, Y.L., Wang, Z.F., Fu, P.Q., Yang, T., Jiang, Q., Dong, H.B., Li, J., Jia, J.J., 2013. Aerosol composition, sources and processes during wintertime in Beijing, China. *Atmos. Chem. Phys.* 13, 4577–4592.
- Ulbrich, I.M., Canagaratna, M.R., Zhang, Q., Worsnop, D.R., Jimenez, J.L., 2009. Interpretation of organic components from positive matrix factorization of aerosol mass spectrometric data. *Atmos. Chem. Phys.* 9, 2891–2918.

- Wang, Q.Q., Sun, Y.L., Jiang, Q., Du, W., Sun, C.Z., Fu, P.Q., Wang, Z.F., 2015. Chemical composition of aerosol particles and light extinction apportionment before and during the heating season in Beijing, China. *J. Geophys. Res. Atmos.* 120, 12708–12722.
- Wang, X., Chen, J., Cheng, T., Zhang, R., Wang, X., 2014. Particle number concentration, size distribution and chemical composition during haze and photochemical smog episodes in Shanghai. *J. Environ. Sci. (China)* 26, 1894–1902.
- Wang, Z., Ding, Y., Zhang, Y., Wang, C., Li, J., Gu, Y., 2012. Feature and mechanism of the Foehn weather on east slope Taihang Mountains I: statistic feature. *Plateau Meteorol.* 31, 547–554.
- Wang, Z.B., Hu, M., Wu, Z.J., Yue, D.L., He, L.Y., Huang, X.F., Liu, X.G., Wiedensohler, A., 2013. Long-term measurements of particle number size distributions and the relationships with air mass history and source apportionment in the summer of Beijing. *Atmos. Chem. Phys.* 13, 10159–10170.
- Wu, Z., Hu, M., Lin, P., Liu, S., Wehner, B., Wiedensohler, A., 2008. Particle number size distribution in the urban atmosphere of Beijing, China. *Atmos. Environ.* 42, 7967–7980.
- Xie, C., Xu, W., Wang, J., Wang, Q., Liu, D., Tang, G., Chen, P., Du, W., Zhao, J., Zhang, Y., Zhou, W., Han, T., Bian, Q., Li, J., Fu, P., Wang, Z., Ge, X., Allan, J., Coe, H., Sun, Y., 2019. Vertical characterization of aerosol optical properties and brown carbon in winter in urban Beijing, China. *Atmos. Chem. Phys.* 19, 165–179.
- Xu, W., Sun, Y., Wang, Q., Zhao, J., Wang, J., Ge, X., Xie, C., Zhou, W., Du, W., Li, J., Fu, P., Wang, Z., Worsnop, D.R., Coe, H., 2019. Changes in aerosol chemistry from 2014 to 2016 in winter in Beijing: insights from high-resolution aerosol mass spectrometry. *J. Geophys. Res.-Atmos.* 124, 1132–1147.
- Xu, W.Q., Sun, Y.L., Chen, C., Du, W., Han, T.T., Wang, Q.Q., Fu, P.Q., Wang, Z.F., Zhao, X.J., Zhou, L.B., Ji, D.S., Wang, P.C., Worsnop, D.R., 2015. Aerosol composition, oxidation properties, and sources in Beijing: results from the 2014 Asia-Pacific economic cooperation summit study. *Atmos. Chem. Phys.* 15, 13681–13698.
- Yue, D., Hu, M., Wu, Z., Wang, Z., Guo, S., Wehner, B., Nowak, A., Achtert, P., Wiedensohler, A., Jung, J., Kim, Y.J., Liu, S., 2009. Characteristics of aerosol size distributions and new particle formation in the summer in Beijing. *J. Geophys. Res.* 114, 1159–1171.
- Yue, D.L., Hu, M., Wang, Z.B., Wen, M.T., Guo, S., Zhong, L.J., Wiedensohler, A., Zhang, Y.H., 2013. Comparison of particle number size distributions and new particle formation between the urban and rural sites in the PRD region, China. *Atmos. Environ.* 76, 181–188.
- Yue, D.L., Hu, M., Wu, Z.J., Guo, S., Wen, M.T., Nowak, A., Wehner, B., Wiedensohler, A., Takegawa, N., Kondo, Y., Wang, X.S., Li, Y.P., Zeng, L.M., Zhang, Y.H., 2010. Variation of particle number size distributions and chemical compositions at the urban and downwind regional sites in the Pearl River Delta during summertime pollution episodes. *Atmos. Chem. Phys.* 10, 9431–9439.
- Zhang, J.K., Wang, L.L., Wang, Y.H., Wang, Y.S., 2016. Submicron aerosols during the Beijing Asia-Pacific economic cooperation conference in 2014. *Atmos. Environ.* 124, 224–231.
- Zhang, R., Wang, G., Guo, S., Zamora, M.L., Ying, Q., Lin, Y., Wang, W., Hu, M., Wang, Y., 2015. Formation of urban fine particulate matter. *Chem. Rev.* 115, 3803–3855.
- Zhang, R.J., Wang, M.X., Fu, J.Z., 2001. Preliminary research on the size distribution of aerosols in Beijing. *Adv. Atmos. Sci.* 18, 225–230.
- Zhao, J., Du, W., Zhang, Y., Wang, Q., Chen, C., Xu, W., Han, T., Wang, Y., Fu, P., Wang, Z., Li, Z., Sun, Y., 2017. Insights into aerosol chemistry during the 2015 China victory day parade: results from simultaneous measurements at ground level and 260 m in Beijing. *Atmos. Chem. Phys.* 17, 3215–3232.
- Zhou, L., 2005. Mining airborne particulate size distribution data by positive matrix factorization. *J. Geophys. Res.* 110.
- Zhou, Y., Dada, L., Liu, Y., Fu, Y., Kangasluoma, J., Chan, T., Yan, C., Chu, B., Daellenbach, K.R., Bianchi, F., Kokkonen, T.V., Liu, Y., Kujansuu, J., Kerminen, V.-M., Petäjä, T., Wang, L., Jiang, J., Kulmala, M., 2020. Variation of size-segregated particle number concentrations in wintertime Beijing. *Atmos. Chem. Phys.* 20, 1201–1216.